Springer

Journal of Mechanical Science and Technology 23 (2009) 3374~3384

Journal of Mechanical Science and Technology

www.springerlink.com/content/1738-494x
DOI 10.1007/s12206-009-0926-y

Strain gradient plasticity based finite element analysis of ultra-fine wire drawing process †

S. M. Byon[1], C. H. Moon[2] and Y. Lee[3,*]

[1]*Department of Mechanical Engineering, Dong-A University, Busan, 604-714, Korea*
[2]*Rolling Technology & Process Control Group, POSCO Technical Research Laboratories, Pohang, 790-785, Korea*
[3]*Department of Mechanical Engineering, Chung-Ang University, Seoul, 156-756, Korea*

(Manuscript Received July 13, 2009; Revised August 24, 2009; Accepted August 26, 2009)

Abstract

Steady-state rigid-plastic finite element analysis coupled with strain gradient plasticity theory has been performed to examine the size effect of material on its plastic deformation behavior and find an optimal semi-cone angle of die which minimizes the drawing energy in the ultra-fine wire drawing process. A stream-line tracing method was adopted to calculate strain component at each element and a strain surface function was introduced to compute the equivalent strain gradient of each element. Introduction of this function enables us to use an established FE code without renewal of its main structure. Hence, the constitutive equation in FE formulation is changed to couple the strain gradient plasticity. A series of FE simulation reveals that significant differences in drawing stress are observed when material size approaches its intrinsic material length. When the strain gradient plasticity theory is reflected on the steady-state FE analysis, the optimal semi-cone angle of the die is reduced by 30%. The variation of optimal semi-cone angle is attributable to considerable increment of homogeneous deformation when the material size reaches its intrinsic material length.

Keywords: Micro wire drawing; Strain surface function; Strain gradient plasticity; Intrinsic material length; Finite element analysis

1. Introduction

Ultra-fine sized wires are in great demand in manufacturing the pins of a semiconductor lead frame (diameter >10 μm) of very large scale integration and the winding coil of a stepping motor (diameter > 1 μm). To enhance the efficiency of very large scale integration and stepping motor, production of much smaller diameter of wire has been required. The key point in ultra-fine wire production is how to reduce the amount of breaking down of wire during the drawing process because frequent breaking down during the drawing process leads to low productivity. The breaking down of wire during drawing depends on various process conditions (semi-cone angle of die, lubrication, drawing speed, reduction ratio, etc.) as well as the material structure and its mechanical properties. If we focus on the process conditions to reduce the amount of breaking down of wire during drawing, we have to analyze the plastic deformation behavior of the material inside the die and the geometric parameters of die using plasticity theory. However, the conventional plasticity theory has a limitation when material size is reduced to fractions of microns. Finite element analysis linked with the conventional plasticity theory simply shrinks the analysis region as the material size is reduced.

Recently, there have been investigations regarding plastic deformation behavior of material when its physical size scales down from tens of microns to a

† This paper was recommended for publication in revised form by Associate Editor Dae-Eun Kim

*Corresponding author. Tel.: +82 2 824 5256, Fax.: +82 2 814 9476
E-mail address: ysl@cau.ac.kr

fraction of microns. In classical mechanics, the strain (or stress) subject to an external loading remains unchanged where the deformation and loading are proportional to each other even though material size is different. If its size is reduced to fraction of microns, the stress in micro-sized material is bigger than that of millimeter-sized material [1-3]. This is called the 'size effect'. The theory that takes into account the size effect during deformation is called the strain gradient plasticity. Important parameters in the strain gradient plasticity, which derive the size effect, are equivalent strain gradient and intrinsic material length of material being deformed.

Hence, if strain gradient plasticity theory is introduced in deformation analysis, the size effect should be reflected on the governing equation, and subsequently we can see the size effect on the deformation behavior. Several studies using finite element method coupled with strain gradient plasticity have been presented. These can be divided mainly into two groups: analysis of micro-indentation [4, 5] and study of crack initiation and propagation [6, 7]. In their studies, displacement-based higher-order continuum theory was adopted to finite element formulation. Since the early strain gradient theory [1-3] involves higher order stress, the equilibrium equation and boundary conditions are essentially complicated, which causes difficulties in obtaining a solution. To overcome this difficulty, Huang et al [8] proposed a method in which the strain gradient effect could be included in analysis using conventional equilibrium equation and boundary conditions. Huang's method gives an accurate solution except at the very near surface of material as much as the method that involves the complicated equilibrium equation and boundary conditions.

In the aforementioned works [1-8], however, FE implementation coupled with strain gradient was carried out by the spatial derivative of element interpolation function, i.e., shape function. This procedure requires much programming effort since it changes the entire parts of the FE formulation. Therefore, an established FE code is useless if one tries to revamp the structure of FE code. Moreover, those approaches based on the elastic-plastic deformation make the analysis complicated since the plastic zone grows during deformation and subsequently, internal elastic-plastic boundaries are obscure. Hence, the algorithmic treatment of internal elastic-plastic boundaries in FE implementations with strain gradient considered is significantly difficult [9]. To overcome those problems, Byon and Lee [10] presented a rigid-plastic based FE approach with strain gradient effect considered.

In this paper, we present a more effective methodology for rigid-plastic FE implementation coupled with strain gradient plasticity in the analysis of the general steady-state metal forming process. For this purpose, the concept of strain surface function is introduced to include the effect of strain gradient into the conventional FE formulation used for metal forming analysis. The advantage of the proposed method is that an established conventional FE code can be used in the analysis of micro-sized material without changing the structure of the main FE program.

We employed rigid-plastic steady-state FE formulation [11] joined with the strain gradient plasticity and applied it to a micro wire drawing process. The characteristic of this FE formulation is that the mesh is fixed since the process configuration does not change with time, and its nodal velocities are solved under given boundary conditions. According to the work-hardening characteristics of the material, these nodal velocities are iteratively updated depending on the elemental strain distribution which is specially calculated. Hence, this method is suitable when the amount of main deformation is very large compared with initial and final deformation such as rolling, drawing and extrusion.

To examine the size effect of material on the semi-cone angle of die and drawing energy, specimens with diameter of 2.0 μm and 20.0 μm are considered. The semi-cone angles selected in FE simulation are 3^0, 5^0, 7^0 and 9^0, respectively. To understand better the variation of optimal semi-cone angle in terms of material size being deformed, we compute the energy components (homogeneous deformation, friction, shear deformation) required in drawing process. We adopt the method of least squares to calculate the strain gradient tensor, i.e., the spatial derivative of strain tensor. This method allows us to determine the strain surface function, which consists of a corresponding element and elements surrounding it. Material used in this study is polycrystalline copper.

2. Strain gradient plasticity

Researchers in early stages tried to investigate the size effect phenomenologically through experiment. They carried out torsion, bending and indentation tests, and focused deformation behavior for microme-

ter-sized and millimeter-sized materials.

Fleck and Hutchinson [1] attributed this size effect to the strain gradient which was not considered in the conventional plasticity and developed a higher order equilibrium equation to reflect the size effect. They introduced a parameter 'intrinsic material length', related it to the unknowns and finally determined the unknowns through experiments. Nix and Gao [2] tried to make a quantitative correlation for this parameter and the properties. Using Taylor's dislocation model [12, 13], they proposed a flow stress equation that contains the strain gradient and intrinsic material length, and proved its accuracy through micro-indentation test. Gao et al [3] extended it to more general type of flow stress equation which includes equivalent strain gradient and intrinsic material length. They finally proposed mechanism-based strain gradient (MSG) plasticity theory. MSG theory [3], however, still includes a higher order equilibrium equation and consequently needs additional boundary conditions to solve the equilibrium equation.

Recently, Huang [8] proposed a modified MSG plasticity model that does not require a higher order equilibrium equation and additional boundary conditions. In this approach, the equilibrium equation and boundary condition are the same with those of conventional continuum mechanics. The difference is that the equivalent strain gradient is included in the constitutive equation. This approach has, however, limitation in application to deformation analysis on the very near surface of material

2.1 Flow stress - dislocation density

Taylor [12, 13] expressed the flow stress at continuum level in terms of several parameters at micro level.

$$\begin{aligned}\bar{\sigma} &= \bar{M}\bar{\tau} \\ &= \bar{M}\alpha\mu\, b\sqrt{\rho} \\ &= \bar{M}\alpha\mu\, b\sqrt{\rho_S + \rho_G}\end{aligned} \tag{1}$$

$\bar{M}$, called Taylor factor, represents a conversion factor between critical resolved shear stress, $\bar{\tau}$ of crystalline slip system and the flow stress, $\bar{\sigma}$. In case of FCC (face centered cubic) metal, $\bar{M} = 3.06$ [8]. α stands for material-dependent constant and μ, b, ρ represent shear modulus, magnitude of Burgers vector and dislocation density. ρ_S represents statistically stored dislocation (SSD) and ρ_G geometrically necessary dislocation (GND). The concept of SSD and GND was first proposed by Ashby [14].

2.2 Flow stress - intrinsic material length

When material size is reduced to micrometer size, its flow stress is described as a function of strain, strain gradient and intrinsic material length. This is a basic principle of strain gradient plasticity and the equation for the flow stress is given in the form [3]

$$\bar{\sigma} = \sigma_{ref}\sqrt{f^2(\bar{\varepsilon}) + \chi\bar{\eta}} \tag{2}$$

where σ_{ref} and $f(\bar{\varepsilon})$ represent reference stress and work hardening function of the yield stress curve obtained from uni-axial tensile test. $\bar{\eta}$ is equivalent strain gradient. χ represents the intrinsic material length and is a parameter which plays a role to make the flow stress dependent upon the material size at micro level.

In one-dimensional deformation, $\chi\bar{\eta}$ in Eq. (2) can be approximated as

$$\chi\bar{\eta} \approx \chi\,(\Delta\varepsilon/\Delta x) = (\chi/\Delta x)\Delta\varepsilon \tag{3}$$

Δx and χ are, respectively, the characteristic length and intrinsic length of material. When Δx has a similar order compared with χ , $\chi\bar{\eta}$ influences the flow stress behavior significantly. But where $\Delta x >> \chi$, $\chi\bar{\eta}$ in Eq. (3) comes close to zero. Hence, Eq. (2) becomes the flow stress equation employed in the conventional plasticity. Huang et al. [8] suggested an explicit form of χ as follows:

$$\chi = \bar{M}^2\bar{r}\alpha^2\left(\frac{\mu}{\sigma_{ref}}\right)^2 b \tag{4}$$

$\bar{r}$ is the Nye factor which represents the average ratio of geometrically necessary dislocation to the most efficient configuration of polycrystalline material [8]. In case of FCC polycrystalline material, $\bar{r}$ is about 1.9. For polycrystalline copper, its mechanical properties and intrinsic material length are listed in Table 1. We know that the size of χ is a few micrometers.

2.3 Flow stress in terms of macroscopic and microscopic parameters

Substituting Eq. (4) into Eq. (2) and comparing with Eq. (1) yields an explicit form of statistically

Table 1. Material constants and intrinsic material length for polycrystalline copper.

Material constants	Symbols	Values
Coefficient of the Taylor's dislocation model	α	0.3
Shear modulus(GPa)	μ	42
Coefficient stress of yield function* (MPa)	σ_{ref}	688
Magnitude of the Burgers Vector (nm)	b	0.255
Intrinsic material length(μm)	χ	1.54

*Yield function for polycrystalline copper was $688\bar{\varepsilon}^{0.3}$.

stored dislocation and geometrically necessary dislocation as follows:

$$\rho_S = \left(\frac{\sigma_{ref} f(\bar{\varepsilon})}{\bar{M}\alpha\mu b} \right)^2 \text{ and } \rho_G = \bar{r}\,\frac{\bar{\eta}}{b} \tag{5}$$

Consequently, the flow stress can be expressed as a function of macroscopic and microscopic parameters. Combination of Eq. (5) and (1) yields flow stress as follows:

$$\bar{\sigma} = \bar{M}\alpha\mu b \sqrt{\left(\frac{\sigma_{ref} f(\bar{\varepsilon})}{\bar{M}\alpha\mu b} \right)^2 + \bar{r}\,\frac{\bar{\eta}}{b}} \tag{6}$$

2.4 Strain gradient tensor and equivalent strain gradient

The strain gradient is defined as twice differentiation of the displacement field:

$$\eta_{ijk} = u_{k,ij} \tag{7}$$

The definition of strain expressed in terms of displacement, $\varepsilon_{ij} = 1/2(u_{i,j} + u_{j,i})$ is differentiated until $u_{k,ij}$ is left. If we change the index notation of it properly, Eq. (7) can be rewritten as

$$\eta_{ijk} = \varepsilon_{ik,j} + \varepsilon_{jk,i} - \varepsilon_{ij,k} \tag{8}$$

Similar to the equivalent strain in the conventional plasticity, the concept of equivalent strain gradient is introduced. The equivalent strain gradient is expressed in terms of three invariants [3].

$$\bar{\eta} = \sqrt{c_1\eta_{iik}\eta_{jjk} + c_2\eta_{ijk}\eta_{ijk} + c_3\eta_{ijk}\eta_{kji}} \tag{9}$$

Application of Eq. (9) to three type of tests, i.e., plane strain bending, pure torsion and axisymmetric void growth experiment yields algebraic equations in terms of $c_1 \sim c_3$. Solving the algebraic equations gives $c_1 = 0$, $c_2 = 1/4$ and $c_3 = 0$ [3]. Therefore, the equivalent strain gradient is

$$\bar{\eta} = \sqrt{\frac{1}{4}\eta_{ijk}\eta_{ijk}} \tag{10}$$

3. Finite element analysis with strain gradient considered

3.1 Boundary value problem with strain gradient plasticity

We have the following boundary value problem applicable to deformation of micro-sized material with the flow stress model (Eq. (6)):

- Equilibrium equation: $\sigma_{ij,j} + F_d = 0$ (11)
- Constitutive equation:

$$\sigma'_{ij} = \frac{2\dot{\varepsilon}_{ij}}{3\bar{\dot{\varepsilon}}} \left[\bar{M}\alpha\mu b \sqrt{\left(\frac{\sigma_{ref} f(\bar{\varepsilon})}{\bar{M}\alpha\mu b} \right)^2 + \bar{r}\,\frac{\bar{\eta}}{b}} \right] \tag{12}$$

where, $\sigma_{ij} = -p\delta_{ij} + \sigma'_{ij}$

- Incompressibility condition: $v_{i,i} = 0$ (13)
- Boundary conditions: $\sigma_{ij} n_j = h_i$ and $v_i = \bar{v}_i$ (14)

F_d represents the distributed force vector acting on entire analysis domain. p, h_i and v_i stand for hydrostatic pressure, traction vector and velocity vector of particle. The strain rate tensor, $\dot{\varepsilon}_{ij}$ is related to the velocity gradient, i.e., $\dot{\varepsilon}_{ij} = 1/2\left(v_{i,j} + v_{j,i}\right)$. $\bar{\dot{\varepsilon}}$ represents equivalent strain rate.

The equilibrium equation can be rewritten in terms of velocity and hydrostatic pressure by substituting the constitutive equation and the strain rate-velocity relation into Eq. (11). Solving this equation with the boundary conditions, we can obtain the velocity and hydrostatic pressure field. The velocity and hydrostatic pressure fields are then substituted for the definition of strain rate, equivalent strain rate, strain and strain gradient.

3.2 Calculation of element strain components in steady-state metal forming

Fig. 1 illustrates a schematic which calculates the components of elemental strain in steady-state metal forming. Solid marks represent the elements at which the strain components are calculated. Empty marks denote elements on the streamline used in strain calculation of the given element. It is shown that streamlines are distinguished by the shapes of mark.

If $\mathbf{x}^k$ is denoted as the current position on the given streamline, a neighboring point $\mathbf{x}^{k+1}$ on the same streamline which is sufficiently close to a point $\mathbf{x}^k$ can be approximately given by

$$\mathbf{x}^{k+1} = \mathbf{x}^k + \mathbf{v}^k \Delta t^k \quad \text{where} \quad \Delta t^k = \frac{\Delta x_s}{v_s^k} \tag{15}$$

$\mathbf{v}^k$ represents the velocity vector at the point $\mathbf{x}^k$. v_s^k stands for its magnitude, and Δx_s denotes a marching step size. Using Eq. (15), a streamline may be traced backward starting from the element center to a point on the inlet boundary.

The element strain components can then be evaluated by integrating the evolution equation along the streamline starting from the point on the inlet boundary, as follows:

$$\varepsilon_{ij}^{k+1} = \varepsilon_{ij}^k + \Delta\varepsilon_{ij}^{k+1} \quad \text{where} \quad \Delta\varepsilon_{ij}^{k+1} = \int \frac{\dot{\varepsilon}_{ij}^{k+1}}{v_s} dx_s \tag{16}$$

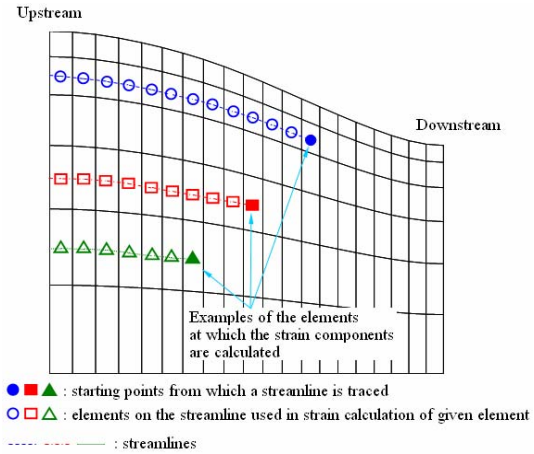

Fig. 1. Conceptual diagram to present the calculation of strain components along streamline.

ε_{ij}^k and ε_{ij}^{k+1} are the strain components at the points $\mathbf{x}^k$ and $\mathbf{x}^{k+1}$, respectively. $\Delta\varepsilon_{ij}^{k+1}$ represents the increment of strain components between $\mathbf{x}^k$ and $\mathbf{x}^{k+1}$, and can be calculated by integrating the components of strain rate, $\dot{\varepsilon}_{ij}^{k+1}$ along the streamline.

Equivalent strain is calculated in the same manner

$$\bar{\varepsilon}^{k+1} = \bar{\varepsilon}^k + \Delta\bar{\varepsilon}^{k+1} \tag{17}$$

$$\Delta\bar{\varepsilon}^{k+1} = \left(\frac{2}{3}\Delta\varepsilon_{ij}^{k+1}\Delta\varepsilon_{ij}^{k+1}\right)^{\frac{1}{2}} \tag{18}$$

It should be noted that the increment of equivalent strain, $\Delta\bar{\varepsilon}^{k+1}$ can also be calculated by the direct integration of equivalent strain rate, $\dot{\bar{\varepsilon}}^{k+1}$ as follows:

$$\Delta\bar{\varepsilon}^{k+1} = \int \frac{\dot{\bar{\varepsilon}}^{k+1}}{v_s} dx_s \tag{19}$$

Since the equivalent strain rate is a scalar quantity, the equivalent strain computed by the direct integration of equivalent strain rate (Eq. (19)) may serve as the benchmark with which the validity of the strain components calculated by Eq. (16) can be examined.

Fig. 2 shows FE meshes and boundary conditions employed for a steady-state wire drawing process. Since the cross section of the wire is circular during deformation, axisymmetric deformation analysis (R-Z coordinates) has been carried out. Symbols A~D stand for points selected for calculating elemental strain components. Elemental strains at points A~D indicate the values integrated along stream line traced. Since axisymmetric deformation is considered, strain components, ε_{RR}, $\varepsilon_{\theta\theta}$, ε_{ZZ}, and ε_{RZ} are calculated.

In Table 2, equivalent strains calculated from strain components (Eqs. (17) and (18)) are compared with those obtained by directly integrating equivalent strain rate (Eq. (19)). Equivalent strains at points

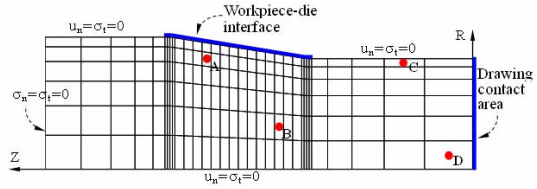

Fig. 2. Boundary conditions and finite element meshes for the analysis of wire drawing. A-D indicate the points where strain components and equivalent strains are calculated for numerical tests.

Table 2. Comparison of equivalent strain ($\bar{\varepsilon}$) calculated from strain components and one directly integrated from equivalent strain rate.

	A	B	C	D
ε_{RR}	-0.0417	-0.1601	-0.1610	-0.1774
$\varepsilon_{\theta\theta}$	-0.0458	-0.1732	-0.1781	-0.1774
ε_{ZZ}	0.0875	0.3333	0.3391	0.3548
ε_{RZ}	0.0884	0.0753	0.0879	0.0341
$\bar{\varepsilon}$ by Eqs. (17) and (18)	0.1671	0.3578	0.4381	0.3593
$\bar{\varepsilon}$ by Eq. (19)	0.1671	0.3578	0.4381	0.3593

A~D calculated from both methods are exactly the same. This implies that we can calculate the strain components by component-wise integration of the components of strain rate (Eq. (16)). We can also observe that incompressibility conditions at points A~D are perfectly satisfied ($\varepsilon_{RR}+\varepsilon_{\theta\theta}+\varepsilon_{ZZ}=0$).

3.3 Strain surface function and calculation of element strain gradient

In this study, we introduce a strain surface function (SSF) to calculate the strain gradient tensor, i.e., the spatial derivative of the strain tensor. The SSF means an analytic surface composed of a group of elemental strain components. To model the analytic surface, we adopt the method of least squares and determine a strain surface function (SSF), which consists of a corresponding element and elements surrounding it (Fig. 3). It is assumed that the distribution of strain along elements is continuous and does not have a radical change. The number of elements surrounding the corresponding element determines the number of elements included in the SSF. A set of elements included in the SSF for the corresponding element is called an "element cluster" hereafter. The number of elements in the element cluster is more than nine. If the number of elements is less than nine, an element layer is added.

As the strain surface function (SSF), we choose a quadratic function as follows:

$$(\tilde{\varepsilon}_{ij})_m = ({}_0\beta_{ij})_m + ({}_1\beta_{ij})_m R + ({}_2\beta_{ij})_m Z + ({}_3\beta_{ij})_m RZ + ({}_4\beta_{ij})_m R^2 + ({}_5\beta_{ij})_m Z^2 \tag{20}$$

$(\tilde{\varepsilon}_{ij})_m$ represents the quadratic function at the mth element and $({}_0\beta_{ij})_m \sim ({}_5\beta_{ij})_m$ coefficients. R and Z

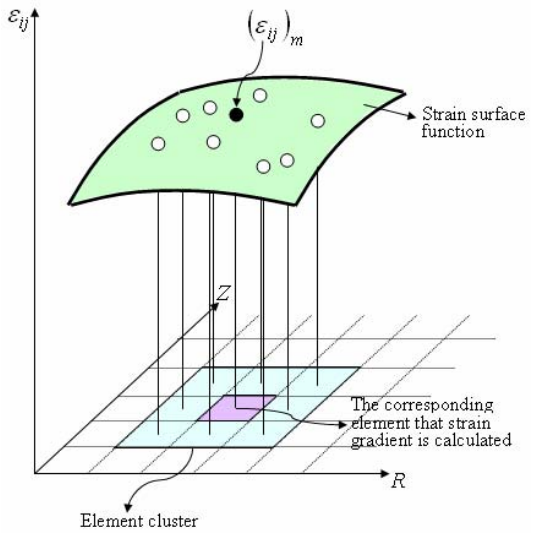

Fig. 3. Schematic diagram of an element cluster and strain surface function of strain components.

stand for coordinates of the element cluster. It is defined the solution of Eq. (20) to be the coefficient $({}_0\beta_{ij})_m \sim ({}_5\beta_{ij})_m$ that minimizes the sum of the square, $(\Psi_{ij})_m$

$$(\Psi_{ij})_m = \sum_{k=1}^{n}\left[(\varepsilon_{ij})_k - (\tilde{\varepsilon}_{ij})_m\right]^2 \tag{21}$$

where, n is the entire number of elements in an element cluster and $(\varepsilon_{ij})_k$ represents the value for strain in the element cluster. In order for Eq. (21) to be minimum, its partial derivatives with respect to $({}_0\beta_{ij})_m \sim ({}_5\beta_{ij})_m$, should be equal to zero.

$$\frac{\partial(\Psi_{ij})_m}{\partial({}_p\beta_{ij})_m} = 0, \quad (p = 0, 1, ..., 5) \tag{22}$$

Eq. (22) is rewritten in a matrix form as follows:

$$\begin{bmatrix} n & \sum R_k & \sum Z_k & \sum R_k Z_k & \sum R_k^2 & \sum Z_k^2 \\ & \sum R_k^2 & \sum R_k Z_k & \sum R_k^2 Z_k & \sum R_k^3 & \sum R_k Z_k^2 \\ & & \sum R_k^2 & \sum R_k Z_k^2 & \sum R_k^2 Z_k & \sum Z_k^3 \\ & & & \sum R_k^2 Z_k^2 & \sum R_k^3 Z_k & \sum R_k Z_k^3 \\ & \text{Symm.} & & & \sum R_k^4 & \sum R_k^2 Z_k^2 \\ & & & & & \sum Z_k^4 \end{bmatrix}$$

$$\begin{bmatrix} ({}_0\beta_{ij})_m \\ ({}_1\beta_{ij})_m \\ ({}_2\beta_{ij})_m \\ ({}_3\beta_{ij})_m \\ ({}_4\beta_{ij})_m \\ ({}_5\beta_{ij})_m \end{bmatrix} = \begin{bmatrix} \sum_{k=1}^{n} (\varepsilon_{ij})_k \\ \sum_{k=1}^{n} R_k (\varepsilon_{ij})_k \\ \sum_{k=1}^{n} Z_k (\varepsilon_{ij})_k \\ \sum_{k=1}^{n} R_k Z_k (\varepsilon_{ij})_k \\ \sum_{k=1}^{n} R_k^2 (\varepsilon_{ij})_k \\ \sum_{k=1}^{n} Z_k^2 (\varepsilon_{ij})_k \end{bmatrix} \tag{23}$$

Solving Eq. (23) gives the coefficients, $({}_0\beta_{ij})_m \sim ({}_5\beta_{ij})_m$ and consequently the quadratic function at the m[th] element, i.e., Eq. (20) is fully determined. Finally, the strain gradient at m[th] element is obtained by differentiating the quadratic function with respect to *R* and *Z*, respectively.

$$(\varepsilon_{ij,R})_m \approx \frac{\partial(\tilde{\varepsilon}_{ij})_m}{\partial R} = ({}_1\beta_{ij})_m + ({}_3\beta_{ij})_m Z + 2({}_4\beta_{ij})_m R \tag{24}$$

$$(\varepsilon_{ij,Z})_m \approx \frac{\partial(\tilde{\varepsilon}_{ij})_m}{\partial Z} = ({}_2\beta_{ij})_m + ({}_3\beta_{ij})_m R + 2({}_5\beta_{ij})_m Z \tag{25}$$

3.4 Computational procedure

In the following, a procedure which analyzes the steady-state wire drawing process using finite element method coupled with the strain gradient plasticity theory and strain surface function (SSF) is described in detail. A flow chart for the procedure is illustrated in Fig. 4.

Step(1) Generate a finite element mesh and prescribe input parameters and boundary conditions for a given analysis domain.

Step(2) Make an initial guess of the equivalent strain $(\bar{\varepsilon})$ and equivalent strain gradient $(\bar{\eta})$.

Step(3) Based on $\bar{\varepsilon}$ and $\bar{\eta}$, compute the flow stress $(\bar{\sigma})$ to evaluate the element stiffness matrix of finite element formulation.

Step(4) Perform the steady-state finite element analysis to obtain nodal velocity as a solution. From the strain rate – velocity relations, calculate strain rate at each element.

Step(5) Trace entire streamlines by predicting sequentially the final positions in all elements through the streamline passing. Sum up the increment of equivalent strains on a given streamline and update the equivalent strains for all elements.

Step(6) To calculate the strain surface function (SSF) and the strain gradient, determine the range of the element cluster. It is based on the nodal connectivity of mesh system used in finite element analysis, as shown in Fig. 3.

Step(7) Apply the method of least squares to the elements belonging to the element cluster and obtain the strain surface function (SSF). The SSF (Eq. (20)) is calculated repeatedly as many as the total number of elements included in analysis domain.

Step(8) Calculate the strain gradient components through differentiating the SSF with respect to *R* and *Z* direction. Each element has the two components of strain gradient in this problem. Compute the equivalent strain gradient at each element using Eq. (10).

Step(9) Perform solution process until the fractional norm of equivalent strain and strain gradient reaches the target. Otherwise, repeat the steps (3)-(8).

4. Results and discussion

In finite element simulation, four different semi-cone angles and two different sizes of input specimen are considered to examine the size effect. A larger semi-cone angle indicates a steeper slope of contact length between material and die with respect to center line. Consequently, the die length decreases as the semi-cone angle increases. We use the abbreviations 'S' and 'L' to distinguish the difference of material size. Material 'S' indicates input specimen with diameter of 2 μm (therefore, its radius is 1 μm in axisymmetric analysis.) and material 'L' input specimen with diameter of 20 μm (thus, its radius is 10 μm in axisymmetric analysis). The background for this choice is as follows. The material selected in the FE simulation is polycrystalline copper and its intrinsic material length is 1.54 μm. Hence 'S' has a strong effect of intrinsic material length during deformation, while 'L' has a weak effect of that. For all cases, the reduction ratio is the same as 29.44% and Coulomb's friction model with the coefficient 0.05 is employed in the analysis.

Fig. 5 shows the R-directional strain distribution (ε_{RR}) during deformation when the semi-cone angle is 3^0 and 9^0 for different material sizes, 'S' and 'L'. For convenience, the analysis domain of material size 'S' is enlarged greatly. Note that results to which the conventional plasticity is applied appear on the right

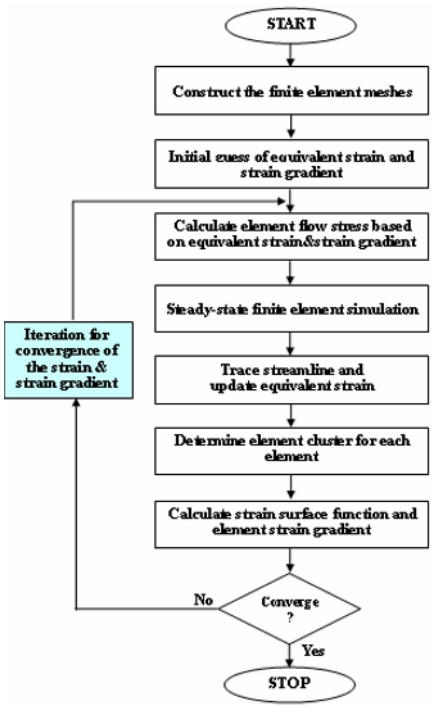

Fig. 4. Flow chart which conducts the steady-state finite element analysis coupled with strain gradient plasticity and strain surface function.

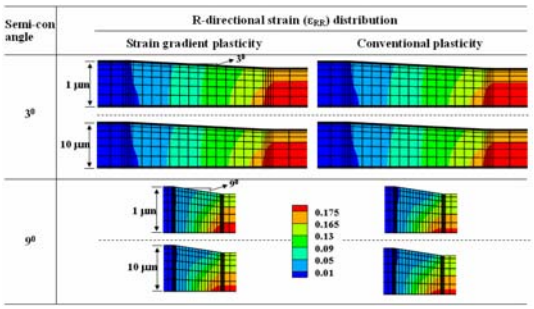

Fig. 5. R-directional strain (ε_{RR}) distribution for different semi-cone angles and analysis methods.

hand side. Results to which the strain gradient plasticity is applied appear on the left hand side. From the viewpoint of strain distribution, almost no variations are observed at the exit if material size 'L' (radius: 10 μm) is deformed. When material size 'S' (radius: 1 μm) is deformed, we can see some differences in strain distribution. The difference is more clear when the semi-cone angle is 9^0 but not so noteworthy. This is by reason that the strain component does not depend on the analysis methods (conventional plasticity or strain gradient plasticity) even though material size and die geometry change somehow.

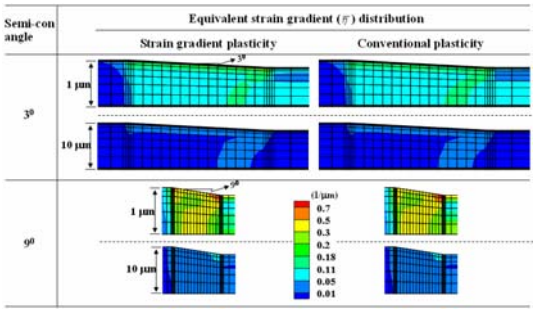

Fig. 6. Equivalent strain gradient ($\bar{\eta}$) distribution for different semi-cone angles and analysis methods.

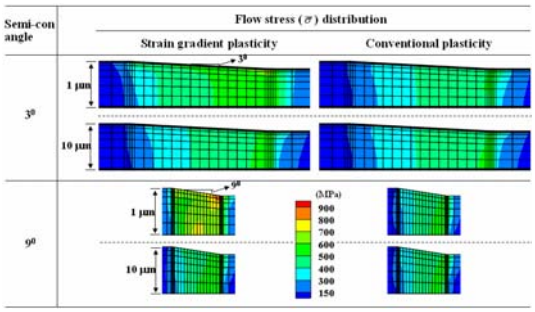

Fig. 7. Flow stress ($\bar{\sigma}$) distribution for different semi-cone angles and analysis methods.

Fig. 6 illustrates the equivalent strain gradient distribution when the semi-cone angle is 3^0 and 9^0 for different material size, 'S' and 'L'. This is calculated on the basis of its definition, Eq. (10) and a series of equations from Eq. (20) to Eq. (25) representing the strain surface functions and its derivatives. The distribution of equivalent strain gradient is different, depending on material size. This is ascribed to the shorter geometric length of material size 'S' than that of material size 'L' when the same amount of strain changes (see Fig. 5). Much more difference is observed when the semi-cone angle is 9^0. But, the analysis methods (strain gradient plasticity and conventional plasticity) do not influence the results since strain and strain gradient are outcomes of geometrical definition. The equivalent strain gradient distribution is reflected in the constitutive equation for the strain gradient plasticity only as noted in Eq. (12).

Fig. 7 shows the flow stress distribution in the material being deformed. When the material size 'L' is deformed in the 3^0 of semi-cone angle, almost no difference is monitored. If the size 'L' is deformed in the 9^0 of semi-cone angle, a small difference is noted. When the material size is reduced to 'S' we can see a distinct difference of flow stress distribution, espe-

cially in case of 9^0 of semi-cone angle which takes more drastic deformation than 3^0 of semi-cone angle. This indicates that size effect is considerable when material size is close to intrinsic material length and deformation is radical due to the geometry of a forming tool.

The flow stress is one of the effective tools for estimating whether the strain gradient plasticity is active or not. The flow stress in Eq. (2) is composed of the deformation resistance by work hardening and the one by strain gradient. The effect of strain gradient on the flow stress is dependent of the characteristic length (Δx) of material relative to the intrinsic material length (χ) as described in Eq. (3). In this problem, the characteristic length is the wire diameter. Since the intrinsic material length is a material constant that is experimentally measured from various tests [8], the characteristic length, i.e., the wire diameter, determines the effect of the strain gradient. As the characteristic length approaches its intrinsic length, $\chi/\Delta x$ comes near 1.0. and then the effect of strain gradient on the flow stress is significant. But if the characteristic length is much larger than the intrinsic length, $\chi/\Delta x$ comes close to 0.0 and therefore the effect of it is negligible. These are unified results deduced from the various mechanical tests by aforementioned studies [1-8]. It should be noted that these results are always applicable to the present micro drawing problem, as shown in Fig. 7.

The effect of material size on an optimal semi-cone angle is examined and results are shown in Fig. 8. The difference in drawing stress between the analysis methods (strain gradient plasticity and conventional plasticity) is summarized in Table 3. When conventional plasticity is used, no difference between material size 'S' and 'L' in the drawing stress is noted. In case of material size 'L', the fact whether strain gradient concept is considered or not influences drawing stress variation little (the maximum difference in drawing stress is 7.6% at semi-cone angle 9^0). However, when material size 'S' is deformed, we can clearly see the effect of material size on an optimal semi-cone angle. In this case, the maximum difference in drawing stress is 58.5% at semi-cone angle 9^0. This result indicates that if the material size is nearly the intrinsic material length, the optimum angle might be changed. This means that we should design again a drawing die with material size decreased so that we can reduce the amount of breaking down of wire during drawing.

Table 3. Differences in drawing stresses calculated from the strain gradient plasticity and conventional plasticity.

Semi-cone angle	Material size(dia.)	Drawing stress(MPa)		Diff. (%)
		SGP*	CP**	
3^0	2.0 μm	305.94	247.99	23.4
	20.0 μm	253.55	247.14	2.6
5^0	2.0 μm	299.76	220.56	35.9
	20.0 μm	229.60	220.20	4.3
7^0	2.0 μm	314.49	212.70	47.9
	20.0 μm	224.98	212.67	5.8
9^0	2.0 μm	342.91	216.32	58.5
	20.0 μm	232.88	216.38	7.6

*SGP represents the strain gradient plasticity.
**CP represents the conventional plasticity.

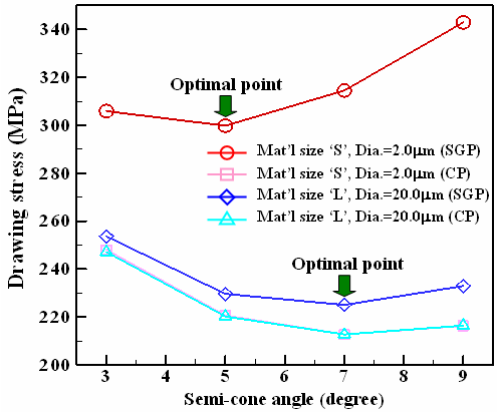

Fig. 8. Variation of drawing stress with material size, strain gradient and semi-cone angle changed. SGP and CP represent the strain gradient plasticity and the conventional plasticity, respectively.

Fig. 9 shows homogeneous deformation energy, friction energy, shear deformation energy required in the drawing process in terms of semi-cone angle for material size 'L'. Total energy is a summation of those energy components. To compare these energies, they are calculated as quantities per unit volume. Solid line indicates energies computed from strain gradient plasticity (SGP) and dashed line energies calculated from conventional plasticity (CP). Almost no difference is observed in friction energy and shear deformation energy. Some differences are visible in homogeneous deformation energy, but the difference is small. Shear deformation energy increases linearly as semi-cone angle does. This is what we have expected. Meanwhile, friction energy is reduced by more than 50% as the semi-cone angle increases from

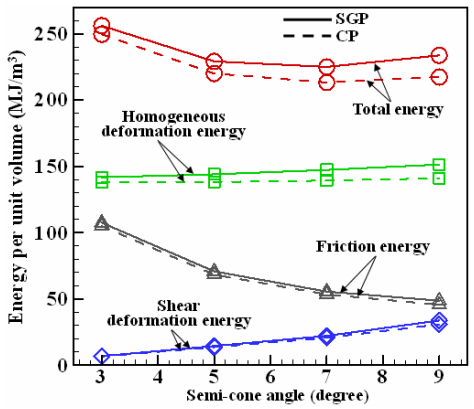

Fig. 9. Composition of drawing energy per unit volume when the incoming wire diameter is 20 μm (Material size 'L'). SGP and CP represent the strain gradient plasticity and the conventional plasticity, respectively.

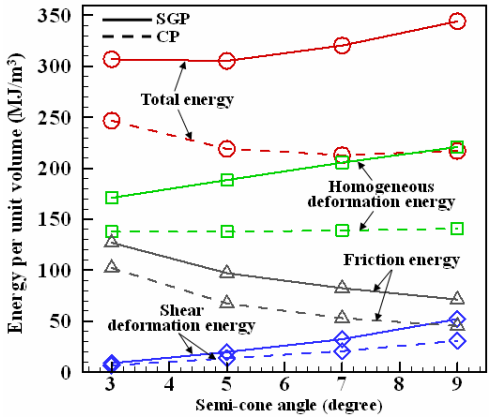

Fig. 10. Composition of drawing energy per unit volume when incoming wire diameter is 2 μm (Material size 'S'). SGP and CP represent the strain gradient plasticity and the conventional plasticity, respectively.

3^0 to 9^0. This is because the longitudinal length of die decreases from 31.2 μm to 10.3 μm as the semi-cone angle increases from 3^0 to 9^0.

Fig. 10 shows homogeneous deformation energy, friction energy, shear deformation energy in terms of semi-cone angle for material size 'S'. When the concept of strain gradient is not reflected in deformation analysis, homogenous deformation energy is practically constant. However, the homogenous deformation energy increases linearly with semi-cone angle increased if the strain gradient theory is considered. This might be attributed to the effect of material size coupled with geometrical configuration, i.e., semi-cone angle, on the homogeneous deformation energy.

Note that the homogeneous deformation energy is calculated from components of normal stresses and normal strains. In conventional plasticity, the homogeneous deformation energy is almost constant regardless of semi-cone angle since the magnitude of these components is dependent on the entry and exit size of the die. However, if material size is reduced to a few micrometers, normal stress components are influenced by strain gradient (See Eq. (12)). The strain gradient is affected by semi-cone angle of die (See Fig. 6). As a result, the homogeneous deformation energy of material size 'S' changes as the semi-cone angle does. Friction energy calculated from strain gradient plasticity is larger than that from conventional plasticity by about 30%. Shear deformation energy along semi-cone angle increases apart from strain gradient plasticity theory. However, its increment is much larger when strain gradient plasticity theory is taken into account. Thus, we can know that the optimal semi-cone angle becomes smaller owing to increment of homogenous deformation energy caused by strain gradient.

5. Concluding remarks

To study the deformation behavior of ultra-fine size material in wire drawing process, we have presented a more effective methodology for the FE analysis of strain gradient plasticity theory in the steady-state metal forming process. We introduced the concept of strain surface function to embrace the effect of strain gradient on the conventional steady-state rigid-plastic FE formulation. The main merit of the proposed approach lies in that the conventional FE code can be used in the deformation analysis of micro-sized material without changing the main structure of the code. Polycrystalline copper (intrinsic material length: 1.54 μm) was used. To investigate the effect of material size on its deformation behavior, specimens with diameter of 2 μm and 20 μm were selected. The conclusions are summarized as follows:

When the material size approaches its intrinsic length the strain gradient becomes significant. If the material satisfying the above condition is deformed plastically, an additional work hardening occurs at the region where the strain gradient is noteworthy. Analysis of energy components (homogeneous deformation, friction energy, shear deformation) during wire drawing reveals that the optimal semi-cone angle of the die changes as material size reaches its intrinsic length. The change of semi-cone angle strongly depends on homogeneous deformation energy.

Results obtained in this study might give impetus on that a wire drawing process designer might have to consider that the optimal semi-cone angle of the die reduces about 30% if material size is close to its intrinsic material length. Analysis method proposed in this study may give an important guideline in computation of mechanical state of material during deformation, not only in wire drawing process but also in various micro deformation process such as micro-forming and micro-machining.

Acknowledgment

This study was supported by research funds from Dong-A University.

References

[1] N. A. Fleck and J. W. Hutchinson, A phenomenological theory for strain gradient effects in plasticity, *Journal of Mechanics and Physics of Solids* 41 (1993) 1825-1857.

[2] W. D. Nix and H. Gao, Indentation size effects in crystalline materials: a law for strain gradient plasticity, *Journal of Mechanics and Physics of Solids* 46 (1998) 411-425.

[3] H. Gao, Y. Huang, W. D. Nix and J. W. Hutchinson, Mechanism-based strain gradient plasticity - I. Theory, *Journal of Mechanics and Physics of Solids* 47 (1999) 1239-1263.

[4] J. Y. Shu and N. A. Fleck, The prediction of a size effect in micro-indentation, *International Journal of Solids and Structures* 35 (1998) 1363-1383.

[5] Y. Huang, Z. Xue, H. Gao, W. D. Nix and Z. C. Xia, A study of microindentation hardness tests by mechanism-based strain gradient plasticity, *Journal of Material Research* 15 (2000) 1786-1796.

[6] Z. C. Xia and J. W. Hutchinson, Crack tip fields in strain gradient plasticity, *Journal of Mechanics and Physics of Solids* 44 (1996) 1621-1648.

[7] Y. Huang, J. Y. Chen, T. F. Guo, L. Zhang and K. C. Hwang, Analytic and numerical studies on mode I and mode II fracture in elastic-plastic materials with strain gradient effects, *International Journal of Fracture* 100 (1999) 1-27.

[8] Y. Huang, S. Qu, K. C. Hwang, M. Li and H. Gao, A conventional theory of mechanism-based strain gradient plasticity, *International Journal of Plasticity* 20 (2004) 753-782.

[9] R. H. J. Peerlings, On the role of moving elastic-plastic boundaries in strain gradient plasticity, *Modelling and Simulation in Materials Science and Engineering*, 15 (2007) S109-S120.

[10] S. M. Byon and Y. Lee, Deformation analysis of micro-sized material using strain gradient plasticity, *Journal of Mechanical Science and Technology*, 20 (2006) 621-633.

[11] S. M. Byon and S. M. Hwang, Process optimal design in non-isothermal, steady-state metal forming by the finite element method, *International Journal for Numerical Method in Engineering* 46 (1999) 1075-1100.

[12] G. I. Taylor, The mechanism of plastic deformation of crystals. Part I – theoretical, *Proceedings of the Royal Society of London A* 145 (1934) 362-387.

[13] G. I. Taylor, Plastic strain in metals, *Journal of the Institute of Metals* 62 (1938) 307-324.

[14] M. F. Ashby, The deformation of plastically non-homogeneous alloys, *Philosophical Magazine* 21 (1970) 399-424.

Sang Min Byon received the B.S. in Mechanical Engineering from Pusan National University, Korea, in 1993. He then received the M.S. and Ph.D. degrees from Pohang University of Science and Technology, Korea, in 1995 and 1999, respectively. Until 2006, he worked as a researcher at POSCO Technical Research Laboratories, Pohang, Korea. He is currently an Assistant Professor in the Department of Mechanical Engineering, Dong-A University, Busan, Korea. He is interested in computational macro and micro analysis in metal forming processes.

Youngseog Lee received the B.S. in Mechanical Engineering from Pusan National University, Korea, in 1989. He then received the M.S. and Ph.D. degrees from Case Western Reserve University, Cleveland, Ohio, USA, in 1992 and 1997, respectively. Until 2003, he worked as a researcher at POSCO Technical Research Laboratories, Pohang, Korea. He is currently an Associate Professor in the Department of Mechanical Engineering, Chung-Ang University, Seoul, Korea. He is interested in computational fracture mechanics and hot rolling process.